Acta Geodyn. Geomater., Vol. 23, No. 1 (221), 1–14, 2026
DOI: 10.13168/AGG.2025.0044
journal homepage: https://www.irsm.cas.cz/acta

ORIGINAL PAPER

INTEGRATED GEOPHYSICAL INVESTIGATION FOR LITHIUM (LI) BEARING PEGMATIC DEPOSITS WITHIN ZURU SCHIST BELTS OF KEBBI STATE, NW NIGERIA

Abdulrahaman Idris AUGIE [1,2,3], Andy Anderson BERY [2] and Ismail Ahmad ABIR[3] *

[1] *Department of Applied Geophysics, Federal University Birnin Kebbi, Nigeria*
[2] *Earth System Processes and Hazard Modeling Center, Geophysics Programme, School of Physics, Universiti Sains Malaysia, 11800 USM, Penang, Malaysia*
[3] *Geophysics Programme, School of Physics, Universiti Sains Malaysia, 11800 USM, Penang, Malaysia*

**Corresponding author's e-mail:* iahmadabir@usm.my

ARTICLE INFO

Article history:
Received 10 July 2025
Accepted 5 September 2025
Available online 11 December 2025

Keywords:
Lithium deposits
Potential mineralised zones
Improved edge detection techniques
Improved hydrothermal alteration techniques
2D geoelectric techniques

ABSTRACT

The present research combined aeromagnetic, aero-radiometric, induced polarisation (IP) and 2D electrical resistivity tomography (ERT) methods to reveal potential lithium-bearing pegmatite minerals of the study area. The datasets of combined airborne magnetic and radiometric data were processed and analysed using improved edge detections and hydrothermal techniques. The results of improved FVD-CET, AS-CET, %K_ratio_eTh, and Ternary grid anomalies reveal regions of major magnetic structures (lineaments), high amplitude magnetic anomalies, and hydrothermal alteration zones associated with the Pan-African Older Granitoid of the basement complex in comparison with the geological setting of the area. Several hydrothermally altered regions with high amplitude magnetic anomaly zones coupled with lineaments were identified to be favourable for lithium-bearing pegmatite minerals. These findings were consistent with previous aeromagnetic studies of the area, which focused solely on magnetic structures rather than alteration zones. Further geoelectric investigation along profiles 1 and 2 revealed three significant zones of lithium-bearing pegmatite mineralisation potential, marked as zones **G**, **L**, and **L1**. These zones are low/high resistivity and chargeability signature regions that could be viewed as probable target areas for lithium mineral exploration. Zones are located in Bajida and Gonan Goli of Kebbi state. The geoelectric approaches yielded a database of accurate coordinates, lateral lengths, and thickness/depths for possible lithium-bearing pegmatite zones. The innovative aspect of this research is the integration of datasets, the use of an improved targeting of hydrothermal alteration techniques, and the creation of a geophysical database for exact locations. These could guide the future exploration programs, supporting sustainable lithium resource development in Nigeria.

1. INTRODUCTION

Lithium-bearing pegmatite was discovered to contain the lightest metal element that exists naturally and it is widely utilised in many different industries for applications like polymers, aeronautics, air therapy, glass, porcelain, ceramics, and medications (Bradley et al., 2017; Wenqing et al., 2023; Balaram et al., 2024). It is specifically used in rechargeable Li-ion batteries, which power increasingly popular electric vehicles in place of fossil fuels (Belgibayeva et al., 2023; Barbosa et al., 2023; Wenqing et al., 2023). Li has been identified as one of the most crucial metals in numerous countries worldwide, and as a result, there is a constant need for Li in the field of low-carbon energy technology (Linnen et al., 2012, 2014; Gourcerol et al., 2019). Thus, Li is necessary to reduce greenhouse gas emissions and build a low-carbon future. Exploring mineral resources, especially Li-bearing pegmatite, requires the use of integrated geophysical methods, particularly gamma-ray spectrometric, magnetic, 2D ERT, and IP techniques to identify the regions of subsurface structures, alterations zones, resistivity, and changeability signatures (Xiaobin et al., 2015; Dzukogi and Mahmud, 2023). Usually, the areas exhibiting these characteristics may be ideally suited for Li-bearing pegmatite (Augie et al., 2022b).

The authors, Bonde et al. (2019), Lawali et al. (2020), Adamu et al. (2021), Lawal et al. (2021), Augie et al. (2022a,b), Augie et al. (2024a,b,c), and Salako et al. (2024), conducted a range of potential field mapping and geochemical analyses to assess the mineralisation potential based solely on aeromagnetic, aero-radiometric, and rock sample data in the study area. Previous qualitative study in the area identified strong lineament/structural tendencies as well as hydrothermal alteration from north to south, and these findings are mainly consistent with the regional structural trend, which is northwest-trending. It also revealed that the basement complex dominates the region, which may be rich in economic minerals. Prominent geochemical properties in a few selected places point to a main far-off hydrothermal source of mineralisation.

However, the area is situated at a low inclined latitude, but none of the earlier studies appropriately

Cite this article as: Augie AI, Bery AA, Abir IA: Integrated geophysical investigation for lithium (Li) bearing pegmatite deposits within Zuru Schist Belts of Kebbi State, NW Nigeria. Acta Geodyn. Geomater., 23, No. 1 (221), 1–14, 2026. DOI: 10.13168/AGG.2025.0044

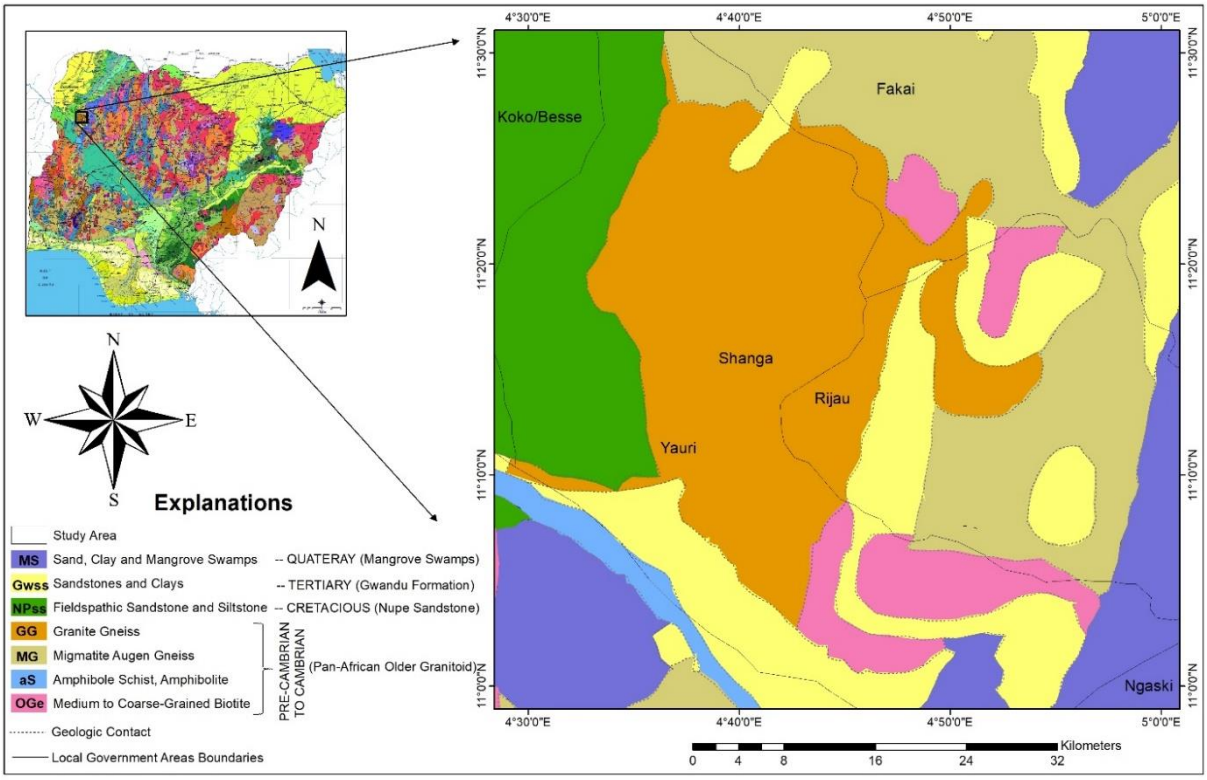

Fig. 1 Location and geological setting of the area (Modified after NGSA, 2006).

applied a filter called reduction-to-equator (RTE), which normally helps in centralising the magnetic anomalies for better interpretation (Augie et al., 2022a,b; Salako et al., 2024). In magnetic data at low latitudes, a certain amplitude must be corrected to avoid spurious noise in the form northern to southern signal results, just like using RTE-filtered data (Holden et al., 2008; Core et al., 2009). The abnormal zones identified in the aeromagnetic and aero-radiometric investigations were not further examined using infield geophysics techniques like 2D ERT and IP methods because the previous research solely used aerial magnetic and radiometric data. In addition, earlier investigations in the area have not used improved edged detection filters such as first vertical derivative combined with centre for exploration targeting (FVD-CET) and analytic signal coupled with centre for exploration targeting (AS-CET) for better lineament detection.

Furthermore, artisanal miners in certain regions of the study area have recently attempted to trace the Li-bearing pegmatite, at Rijau (Dukku) and Shanga. This pegmatite usually occurs as a primary deposit in certain regions of the Zuru Schist belt. The artisanal miners employ a strategy of trial-and-error mining that renders it almost impossible to identify the zones containing these Li minerals. The method of trial-and-error approach has led to the formation of abandoned trenches and pits, which have facilitated environmental pollution. Low yields have also been the consequence of inadequate geophysical studies and a database of exact coordinates.

In this study, integrated geophysical methods involving aeromagnetic, aero-radiometric, 2D ERT, and IP techniques were used to identify subsurface structures, alteration zones, resistivity, and chargeability signature zones within the research region. These features could be important for the exploration of mineral resources, particularly Li-bearing pegmatite minerals. The research commenced with a reconnaissance investigation that utilised high-resolution (HR) aeromagnetic and aero-radiometric data of the research area, in order to reveal structures and alteration zones that can trap riches in minerals. in view of the Li-pegmatite exploration target. As a follow-up geophysical technique, the 2D ERT and IP techniques revealed further details on Li-bearing pegmatite zones and other lithological boundaries. The novel aspect of the research is the use of; integrated geophysical methods, enhanced edge filter techniques, and improved techniques for detecting hydrothermal alteration.

The study area lies between 4°30′0″E and 5°0′0″E longitudes, and latitudes 11°0′0″N and 11°30′0″N. The region comprises the following locations: Fakai, Rijau, Shanga, and Yauri (Fig. 1). According to geology, the area is located between northwest Nigeria's basement complex zones and the Sokoto basin of the sedimentary basin. These include the Pan-African Older Granitoid of the foundation complex, the Gwandu Formation of the Sokoto Basin, and the Nupe Sandstone. As shown in Figure 1, these included sands, clays, fieldspathic, sandstones, siltstones, mangrove swamps, medium to coarse-

grained biotite, migmatitic Augen gneiss, and granite gneiss. Table 1 included both the borehole log and the stratigraphic setting of the area.

2. MATERIALS AND METHODS

2.1. AIRBORNE MAGNETIC METHOD

The aeromagnetic data sheet 96_Shange, which covered the study region, was used in the present study. Fugro conducted an airborne survey in 2009 for the Nigerian government's NGSA. The conditions and parameters set up for the data collection by the Fugro airborne survey are: (a) altitude of 100 m, (b) tie line spacing of 2000 m, and (c) a flight line spacing of 500 m aligned NW –S. The maps are half-degree sheeted and have a 1:100,000 scale. Of all the aforementioned parameter and data collection settings, the dataset defined is high resolution aeromagnetic (HRAM), which is typically used to map shallower subsurface causative bodies.

The main/core field was used for removing the geomagnetic gradient (International Geomagnetic Reference Field, IGRF) in order to correct the obtained data from regional field. The magnetic anomaly (TMI anomaly) is calculated by subtracting the grid values (TMI) from the generated core fields (DGRF for the epoch period).

The TMI corrected anomaly grid has been filtered and reduced to the magnetic equator in order to highlight a magnetised body anomaly, which is typically dependent on the body's orientation in relation to the north magnetic pole, inclination, declination, and local earth's field. Geosoft (Oasis Montaj), Arc GIS, and Surfer tools were used to handle and analyse the data using improved FVD-CET and AS-CET techniques.

The FVD-CET approach helps attenuate long-wavelength magnetic anomalies within the field, which is useful for enhancing closely spaced resolution and resolving attenuate long-wavelength magnetic anomalies inside the field, which is useful for enhancing closely spaced resolution and overlaid anomalies. These anomalous zones may showcase the Location of essential geological formations/structures. The AS-CET amplified the variation in magnetisation of the magnetic sources in the area and indicated the edges of anomalous texture. These variations in magnetisation may be influenced by different earth materials as well as different mineralised zones, particularly metallic minerals such as lithium-bearing pegmatite. CET reveals linear structures (lineament), and these structures can define faults, fractures, or shear zones that represent mineralisation veins.

The anomaly in FVD is much narrower and more nearly matches the width of the magnetic rock body that caused it; the derivatives are given in Equation (1) (Roest et al., 1992). These techniques have been improved in this research by linking with CET (FVD-CET) to reveal structural features, which as well showed the location of the result.

$$L(r) = r^n \tag{1}$$

where *n* order of differentiation.

The amplitude of the analytical signal (AS) can now be established (Pham et al., 2020) using Equation (2). In this study, the estimation was used with the analytical signal coupled with the CET (AS-CET) approach to highlight important zones of lineament. This was further linked to ArcGIS, which revealed more information about the area's location.

$$|AS(x,y,z)| = \sqrt{\left(\frac{\partial T}{\partial x}\right)^2 + \left(\frac{\partial T}{\partial y}\right)^2 + \left(\frac{\partial T}{\partial z}\right)^2} \tag{2}$$

where *x*, *y*, *z* are the directions of total magnetic field and *AS* (*x*, *y*, *z*) is the amplitude of the analytic signal at (*x*, *y*, *z*); *T* is the observed magnetic field at (*x*, *y*, *z*).

2.2. AIRBORNE RADIOMETRIC METHOD

In this study, the aero-radiometric datasets from sheet 96_ Shanga were utilised. These datasets were also collected under the same survey conditions as the previously mentioned aeromagnetic data, and they were similarly obtained from the NGSA, collected by Fugro airborne survey on behalf of Nigeria's Federal Government (FGN).

The Geosoft "Oasis Montaj Software" was utilised to process each radio element using the gridded data that was obtained. This data included the concentrations of Thorium (eTh), Potassium (K), and equivalent Uranium (eU). Each of the three components—%K, eTh, and eU—was blended independently using the blending method provided by the Grid and Image geosoft extension (GX). This resulted in anomalous concentration grids for each element. Equation (3) was utilised to develop the Potassium Ratio Thorium (% K_ratio_eTh) grid anomaly through the use of the Oasis Montaj Grid Math expression builder.

Following that, the total count map integrating the combined effects of radio elements was obtained using the blending method in Grid and Image of GX. These were then used to generate the ternary map, which was created by giving each of the abundances of radio elements a colour. The ternary map is used to identify variations in radio elements that are associated with zones of hydrothermal alteration that may be favourable for the mineralisation of Lithium-bearing pegmatite.

$$H_0 = \frac{h_1}{h_2} \tag{3}$$

where h_1 is %K and h_2 is eTh.

2.3. ELECTRICAL METHOD

The 2D geoelectrical survey involving electrical resistivity and induced polarisation (IP) was also carried out at the Fakai/Rijau boundaries of Kebbi and Niger states, NW Nigeria. Using a dipole-dipole arrangement and a minimum electrode spacing (a) of 10.00 m, 520 m^2 fields were investigated. Based on the

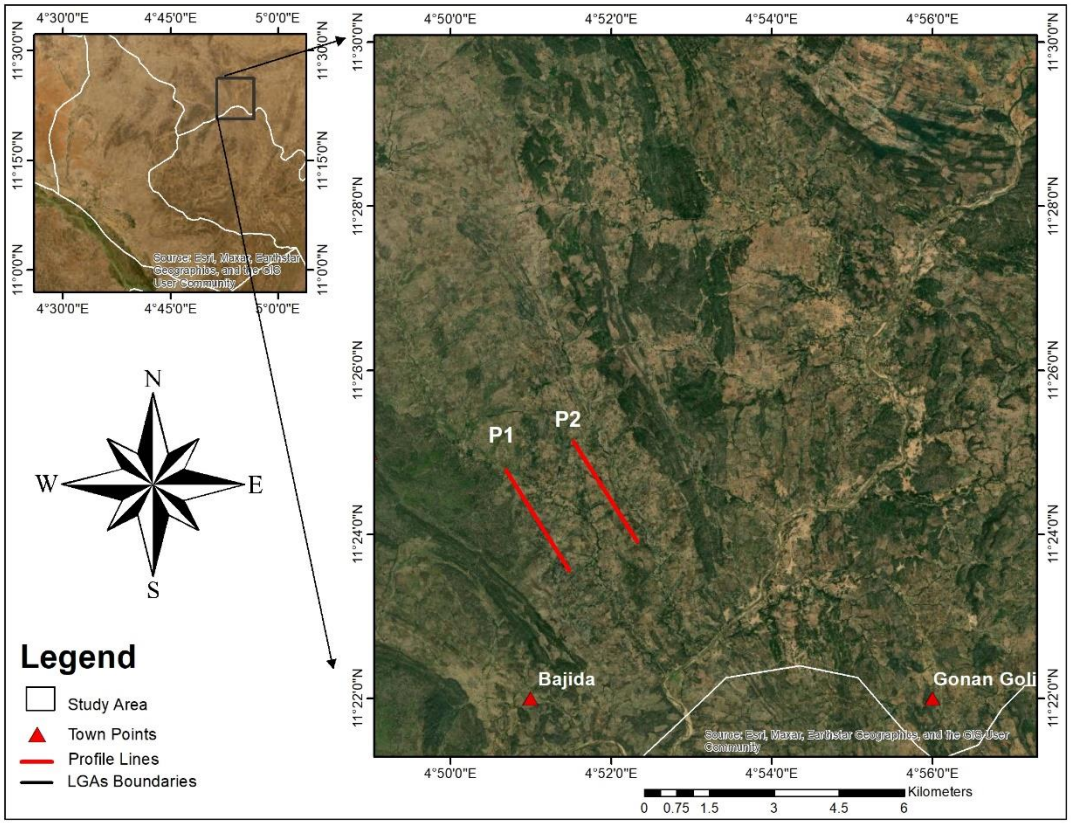

Fig. 2 Layout of the profile lines.

results of aeromagnetic and aero-radiometric techniques, a total of two NW-SE-oriented profiles were created for each 300 m along the profile (Fig. 2). A Super Sting resistivity meter, which was powered by a 12 V battery and attached to an electrode selector, was used to gather the data. This device is capable of measuring IP data and apparent resistivity at the same time. The transmitter that comes with it has automatic/user-configurable currents in milliamperes, which range from 1, 2, 5, 10, 20, 50, 100, 200, 500, and 1000 mA. Two pairs of current electrodes, designated C1 and C2, and two pairs of potential electrodes, designated P1 and P2, would be equally spaced. The separation that separates C1-C2 and P1-P2 is expressed as the product of an integer n, and was used to compute the dipole separation factor or the distance between C1 and P1.

After being initially set to one (1), the dipole separation factor n was raised to two (2), three (3), and so on until it reached its maximum value of eight (8). As a result, measurements have been made of two parameters: the dipole separation factor (n) and the distance between the current electrode pair (*a*). Electrode separation of 10 m was used for the measurements, and n was initially set to 1, 2, 3, and up to 8 (Fig. 3). The greater n increases, the electrode spacing increases correspondingly and the more injected current descends to greater depths. (Loke, 2000).

For the first measurement, electrodes 1, 2, 3, and 4 (C1, C2, P1, and P2) were utilised. At 0 m, C1 was used, P1 at 20 m, C2 at 30 m, and P2 at 30 m. Similarly, in the second measurement, C1 was measured at 20 meters, P1 at 30 meters, P2 at 40 meters, and C2 at 50 meters. The 1×a, 2×a, 3×a, 4×a, 5×a, 6×a, 7×a, and 8×a spacing between C1 and P1, for 'a' is 10 m, were used to repeat these procedures down the profile line. The measured ground apparent resistivity and IP values were acquired at each measurement. The RES2DINV program developed by Loke (1999) was used to analyse the acquired data. It generates IP and 2D resistivity models for the subsurface automatically.

3. RESULTS AND DISCUSSION

3.1. RESULTS OF AIRBORNE MAGNETIC ANALYSIS

The aeromagnetic method was initially employed in this study for a reconnaissance survey. The following processing methods were used: total magnetic intensity reduced to the magnetic equator (TMI-RTE), FVD-CET, and AS-CET

3.1.1. TMI-RTE RESULT

Figure 3 is the resultant composite colour that depicts TMI-RTE anomalies. The red or pink anomalies, which range in value from -636.32 nT to -564.48 nT, are indicative of high magnetic trend anomalies. These areas are located at the Yauri and the

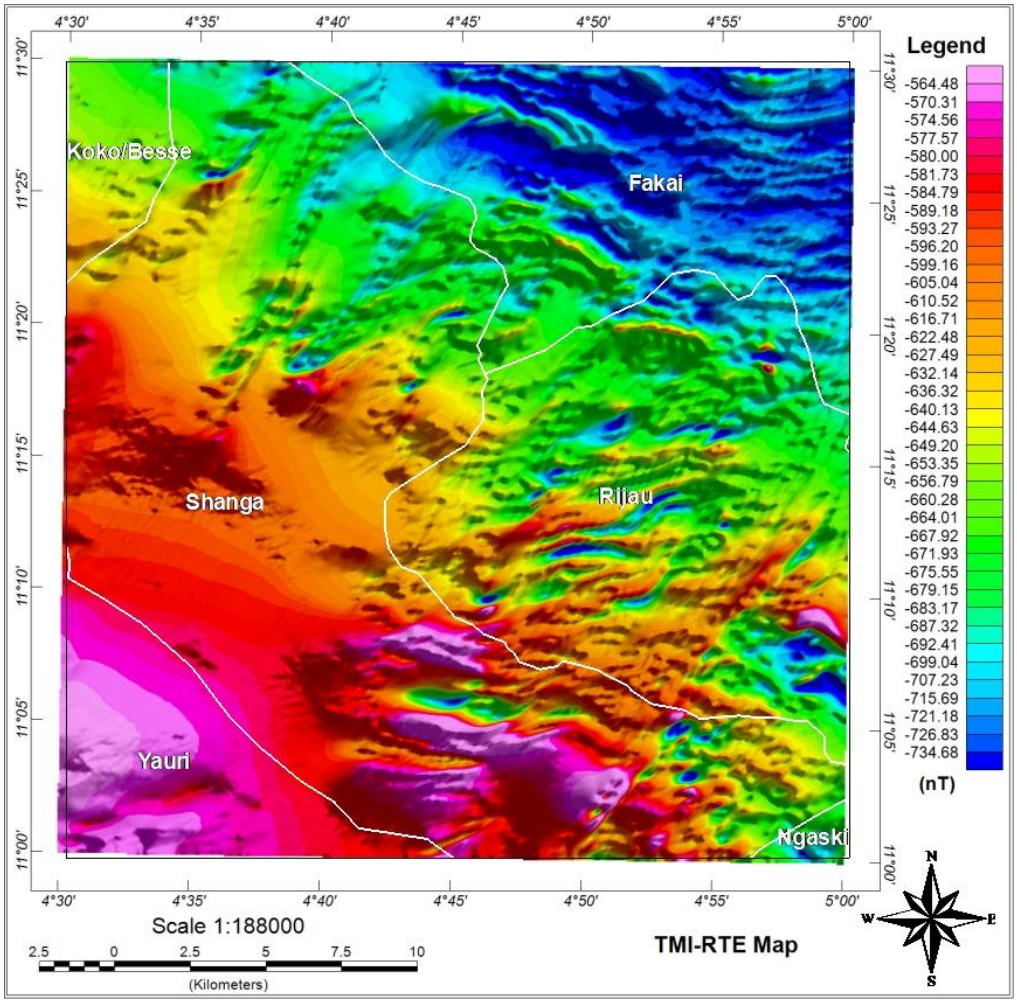

Fig. 3 TMI-RTE map of the study area.

southwest regions of Shanga and Rijau. Low magnetic anomaly areas, which range from -734.68 nT to -656.79 nT, are shown in blue or green. These zones coincide with NE Shanga, Rijau, and Fakai.

As a result, distinct rock formations (Fig. 1) in low and high regions lead to differences in the rocks' magnetic susceptibility in the respective regions. Normally, the susceptible rocks are found at lower depths compared with that of the Curie isotherm, and these are due to the fact that the magnetic equator is a zone of no inclination. Figure 3 shows that the horizontal component of the Earth's magnetic field polarises all rocks in opposition to their magnetisation; large negative values indicate high magnetic susceptibility zones. After subtracting the crustal field and other temporal effects from the measured field, the resulting anomaly over magnetic materials is usually negative (Fig. 3).

3.1.2. FVD-CET LINEAMENTS RESULT

Figure 4 presents the FVD-CET map, which helps to improve closely spaced resolution and superimposed anomalies by attenuating long-wavelength magnetic anomalies within the field. These anomalies were previously invisible in Figure 3's TMI-RTE map. Certain regular linear structures shown in Figure 4 may be thought of as lineaments that suggest fractures, faults, and joints. These lineaments were found in the eastern region of Shanga, Fakai, and Rijau.

As observed in Figure 4, the resulting lineaments fall beneath the edge of the magnetic source and could be faults, fractures, or shear zones, which are commonly utilised as channels for mineral deposits during hydrothermal processes. The features that regulate the mineralisation pattern, especially in the study area's lithium-bearing pegmatite, are the combination of these structures. The areas are underlain by granite gneiss, migmatitic augen gneiss, medium to coarse-grained biotite, sands, clays, fieldspathic, and sandstones, in contrast to the related geological setting. These characteristics and formations could serve as possible mineral hosts.

3.1.3. AS-CET RESULT

The resulting analytic signal map, as seen in Figure 5, highlights the variations in the magnetic anomalours for magnetisation and shows the extent of the anomalous texture. Upon closer inspection of the map, the amplitude is significant along the edge of the

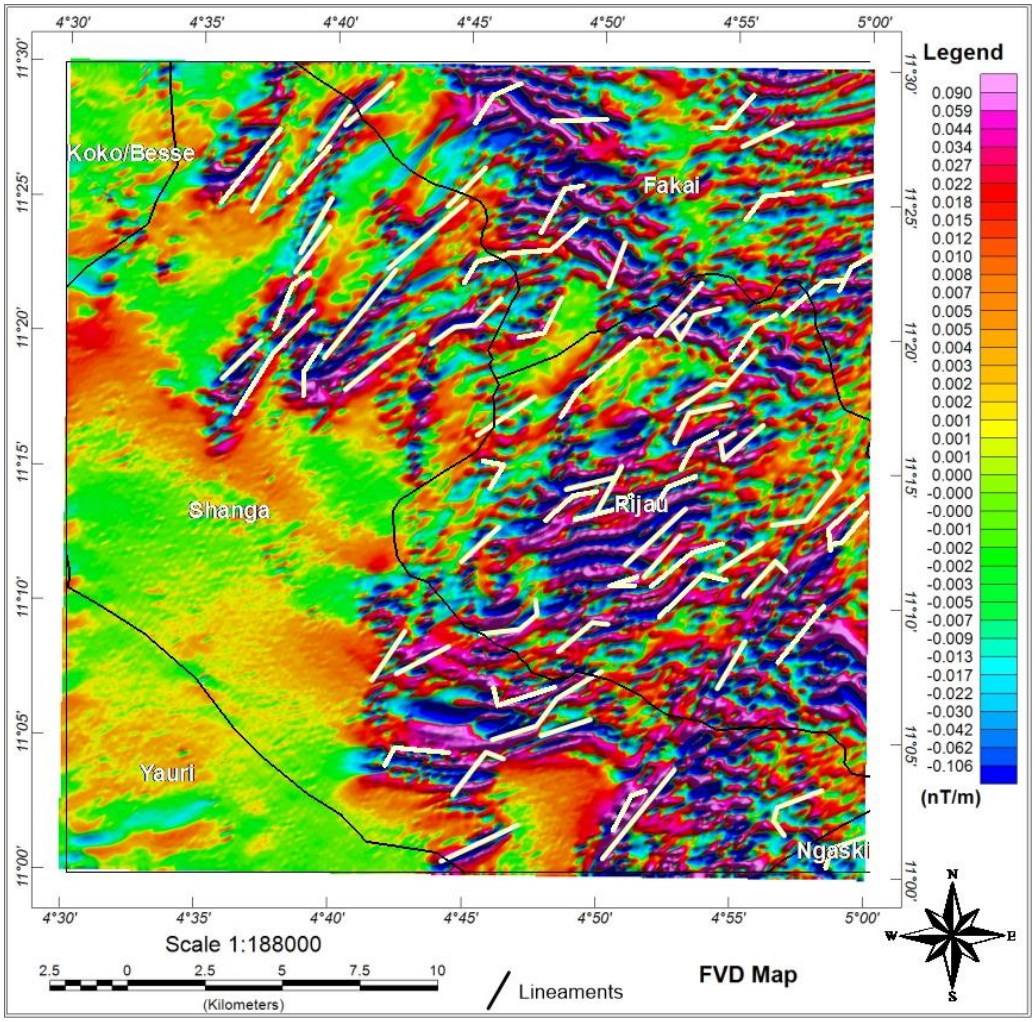

Fig. 4 FVD-CET lineament map of the study area.

magnetic features (lineaments) because of the magnetic variations surrounding the areas that could be associated with the existence of metallic minerals such as lithium-bearing pegmatite. Three distinct magnetic zones were shown on the map: low, moderate, and high, each with a different colour aggregate.

The low magnetised zones are marked in blue having amplitudes that vary between 0.001-0.006 nT/m, moderate in green-yellow with amplitudes ranging from 0.007-0.025 nT/m, and abundant in pink with an amplitude above 0.026 nT/m. When compared to the local geology, the low magnetic susceptibility zones (highlighted in blue) at Koko/besse, the southwest regions of Shanga and Yauri, were linked to laterites, sandstones, siltstones, clay shales, and limestone. These sediments within a zone of low magnetic susceptibility may be significantly influenced by the amount of carbonate in the environment that is being formed. Furthermore, the carbonate species typically rely heavily on the provenance of the sediment as well as the sedimentary facies.

The zones that are coloured green or yellow and exhibit a moderate magnetic anomaly correspond to biotite being coarse-to-medium-grained in contrast to the local geological context (Fig. 1). Zones **J**, on the other hand, were identified as having the maximum amplitude and were shown in pink and these areas are linked to medium to coarse in texture biotite, migmatitic augen gneiss, and granite gneiss in relation to the area's geologic setting.

The high amplitude magnetic anomaly regions (zone **J**) are located in Rijau, the eastern parts of Shanga, and Fakai. Given that zone J exhibits higher magnetic susceptibility comparing the geological context to area (Fig. 1), the type of rock formations highlighted in those areas may play a major role in identifying the species of lithium-bearing pegmatite associated with the rise in minerals that contain oxidised iron.

3.2. RESULTS OF AIRBORNE RADIOMETRIC ANALYSIS

3.2.1. K/ETH RESULT

A map of the % K/eTh concentration ratio is shown in Figure 6, which shows zones of hydrothermally altered zones that usually result in radioactive element enrichment. According to the % K/eTh ratio map, a high concentration of Thorium

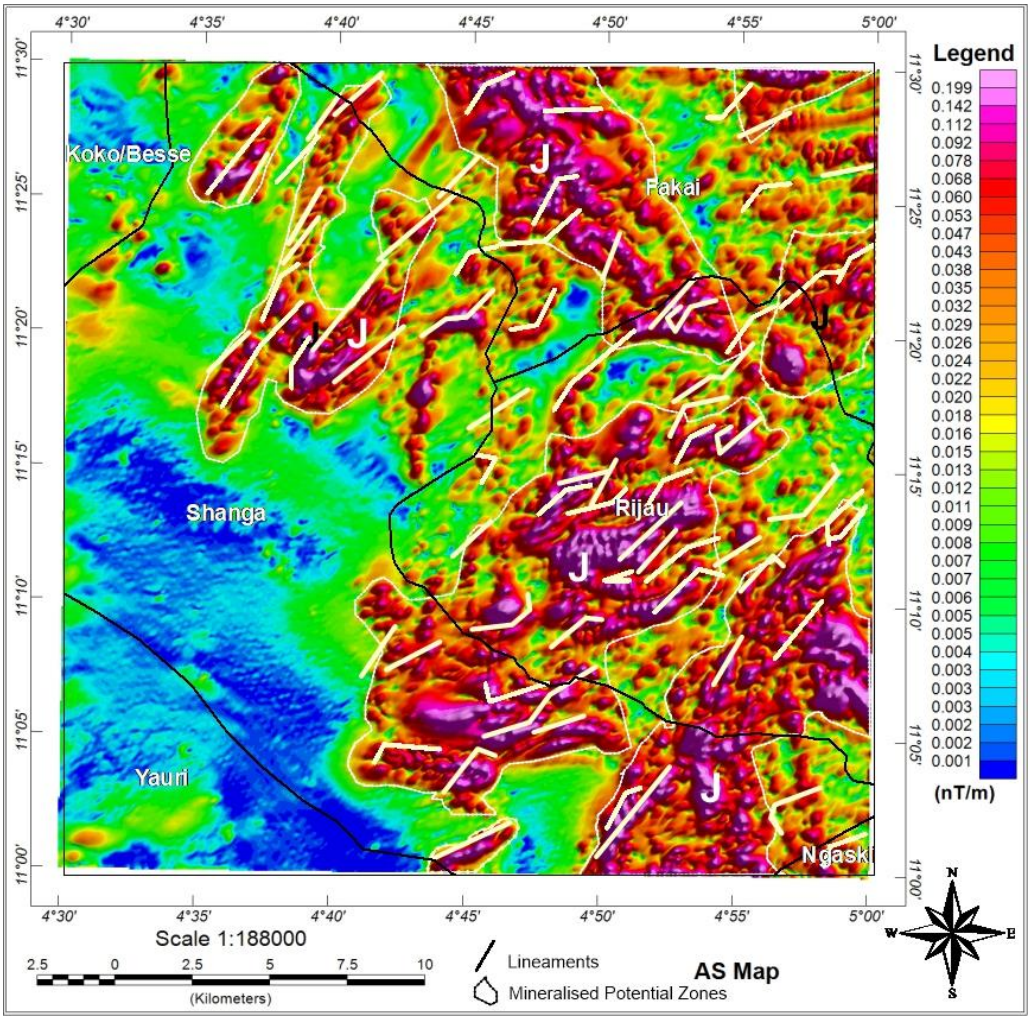

Fig. 5 AS-CET lineament map of the study area.

in the blue colour indicates a level of Thorium, while a high content of Potassium in the red colour indicates a low level of Thorium. Zone J exhibits significant hydrothermally altered zone indications, with values ranging from 0.115 to 0.256 ppm. This zone is associated with high K/Th concentrations and can be found in the following areas: NE parts of Shanga as well as SW parts of the Fakai and Rijau.

Nonetheless, research conducted by Dickson and Scott (1997), Hoover and Pierce (1990), Durrance (1986), and Salako et al. (2024) has demonstrated that the environment's alteration brought about by hydrothermal solutions can decompose and convey a wide variety of minerals and metallic substances, all of which are essential to the mechanisms underlying ore deposition, especially metallic minerals. For this, the hydrothermal alteration zones depicted in this study area may typically accumulate various mineralisation deposits, particularly lithium-bearing pegmatite.

3.2.2. HYDROTHERMAL REGIONS ON TERNARY IMAGES

Figure 7 depicts a ternary radioelement map made up of % K, eTh, and eU in a variety of colour combinations. The red colour represents a high % K (low eU and eTh), with low percentages of K and eTh, the blue colour indicates a significant concentration of eU, and the appearance of green indicates a high eTh concentration (low % the value of K and eU). Cyan represents a high eTh and eU (low % K), Magenta has low eTh and significant % the value of K and eU, Yellow has a high percentage K with low eTh and eU, Black a low percentages of K, low eTh, and low eU and White has high eTh, eU, and % K. Numerous reputable studies, including Hoover and Pierce (1990), Ohioma et al. (2017), Lawal et al. (2021) and Adetona et al. (2022) have found that radioelements that could be used to identify mineralisation potential especially lithium pegmatite through aero-radiometric surveying techniques, with potassium being the most accurate indicator.

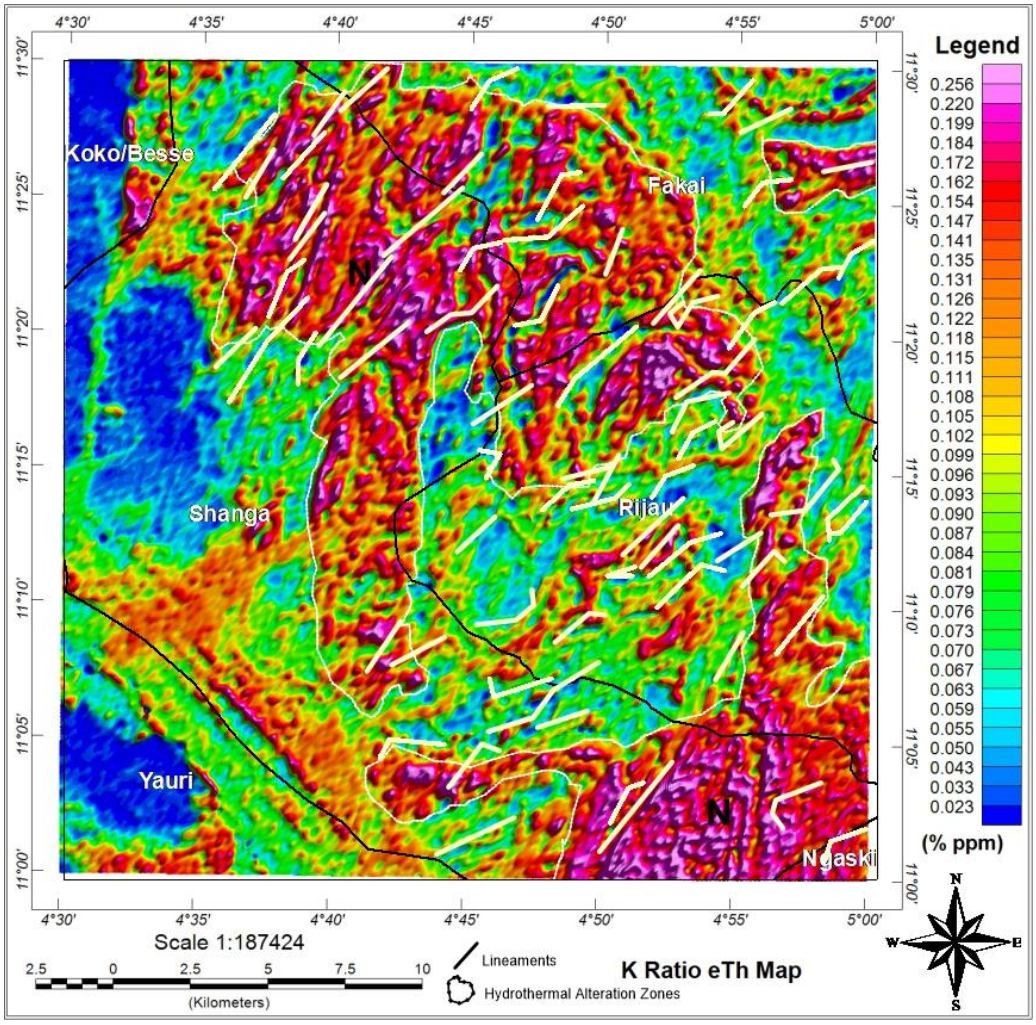

Fig. 6 K ratio eTh coupled with CET lineament map of the study area

According to Figure 7's colour scheme, the area with Blue, Green, Cyan, Yellow, and Black concentrations has extremely low potassium levels, suggesting that hydrothermal alteration did not take place there. However, zone **M** represents a high concentration of Potassium (%K) at 0.118 to 0.256 ppm, but has very low concentrations of eU and eTh, which range from 0.023 to 0.099 ppm as illustrated in Figure 6. These zones are found in the NE regions of Shanga as well as the SW regions of the Fakai and Rijau, and they correlate with the high % K/eTh in the **N** region of the % K/eTh ratio map displayed in Figure 6. The excess Potassium relative to the other elements, particularly Abrasiveness on Thorium, suggests hydrothermal alteration coupled with major magnetic structures (lineaments) could potentially be favourable for lithium-bearing pegmatite minerals. The hydrothermally altered zones **M** and lineaments identified by aero-radiometric and aeromagnetic techniques were investigated further using 2D ERT and IP detailed geophysical methods.

3.3. RESULTS FROM GEOELECTRIC METHODS

In this study, the geological setting of the region influences how the 2D geoelectric-modelled sections are interpreted. Table 1 displays the borehole lithology of the study area, which was furnished by RUWASA (Rural Water Supply and Sanitation Agency), together with resistivity values from previous investigations conducted in the same basement complex (Osazuwa and Chii, 2010; Augie et al., 2024b) were utilised to correlate the results of the survey.

3.3.1. GEOELECTRIC SECTIONS FOR PROFILE 1

The resistivity section of the 2D inverted model for profile 1 is shown in Figure 8(a). The latitudes of the profile are in between 11°24'18.36"N to 11°23'15"N, and longitudes 4°50'58.92"E to 4°51'44.28"E (see Fig. 1). It has a linear distance of 300 meters and is positioned in the northwest to southeast direction. Four distinct zones—**G**, **H**, **L**, and **Q**—were used to section the subsurface feature of the profile. Zone **G** is defined as having resistivity values

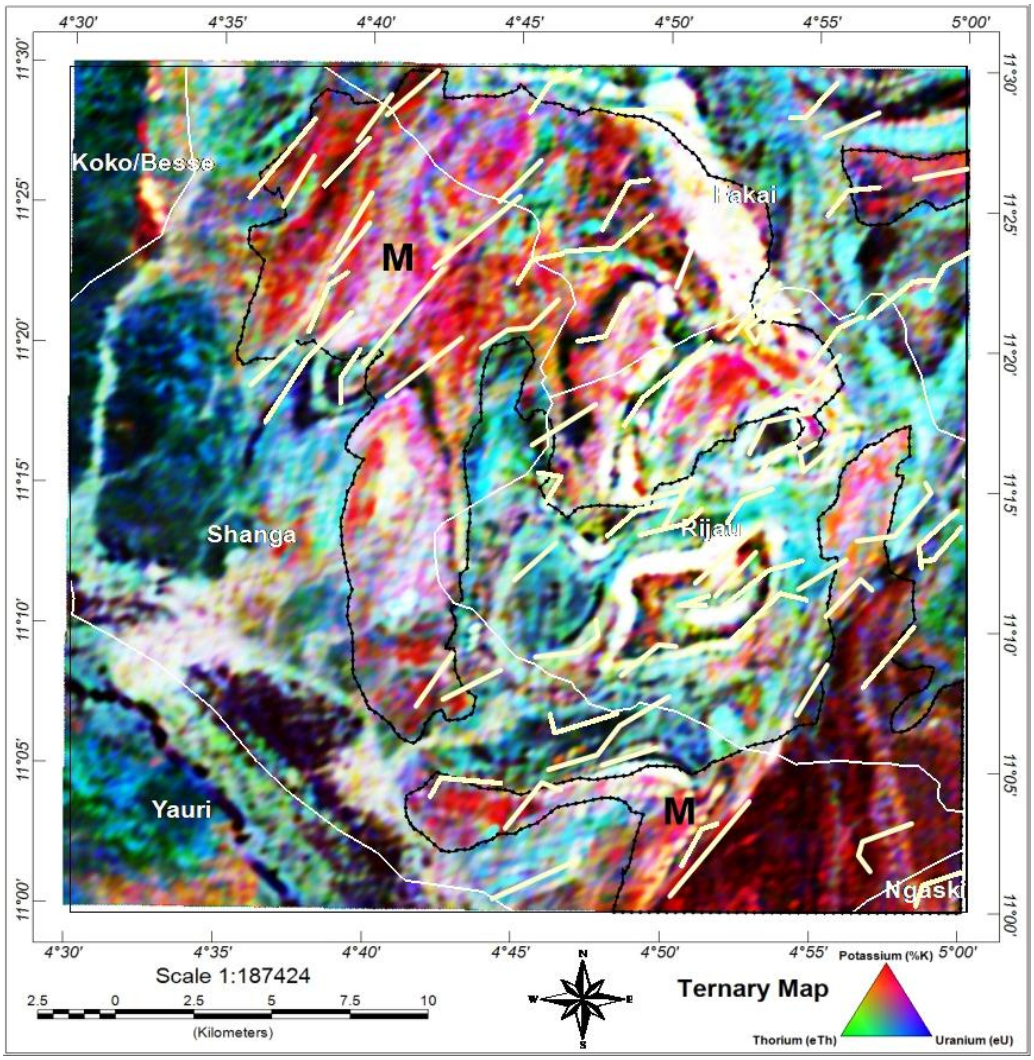

Fig. 7 Ternary map superimposed on CET lineament map of the study area.

Table 1 The study area borehole/lithology log (SARDA, 1988; Augie et al., 2024b)

Lithology	Depth (m)	Thickness (m)	The variation of resistivity (Ωm)
Lateritic Sandy soil	0-2	2	60-1000
Highly Decomposed Quartz's Mica Schist	2-10	8	10-500
Partially Decomposed Quartzite	10-15	12	100-1000
Granite, Quartzite's and Gneiss	15-21	16	200-100000

between 4.009 and 64.8 Ωm, which are spread out over 0-80 m across the profile and measure 12.8 meters in depth and thickness. **H** spans an area of 0-80 m in length and 12.9-24.9 m in thickness, with resistivity values ranging from 64.9 m to 1026 m. Zone **L** is defined by resistivity measures ranging from 1027 Ωm to 4083 Ωm. It spans the following profile lengths: 140–170 m, 180–210 m, and 230–275 m, as well as depths and thicknesses of 23.9 m, 13.8 m, and 8.5 m. Similarly, zone **Q** has a resistivity ranging from 4084 Ωm to 64650 Ωm, and it has taken up space along lengths of 80-140 m and 220-260 m with comparable thicknesses of 18.5-24.9 m and 24.9 m, respectively.

Comparing features zones **G**, **H**, **L**, and **Q** with Table 1 indicates that the subsurface lithology may include quartzite/gneiss, partially decomposed Granite and Quartzite, lateritic soil, and severely decomposed quartz schist. On the other hand, zone **G** of low resistivity areas might be attributed to water persisting in the oxidized rock. This oxidized rock formed from Rhyolite or Granite may help some minerals, especially lithium-bearing pegmatite. Zone **L** is linked to dykes made of Guartzite and Granite that have

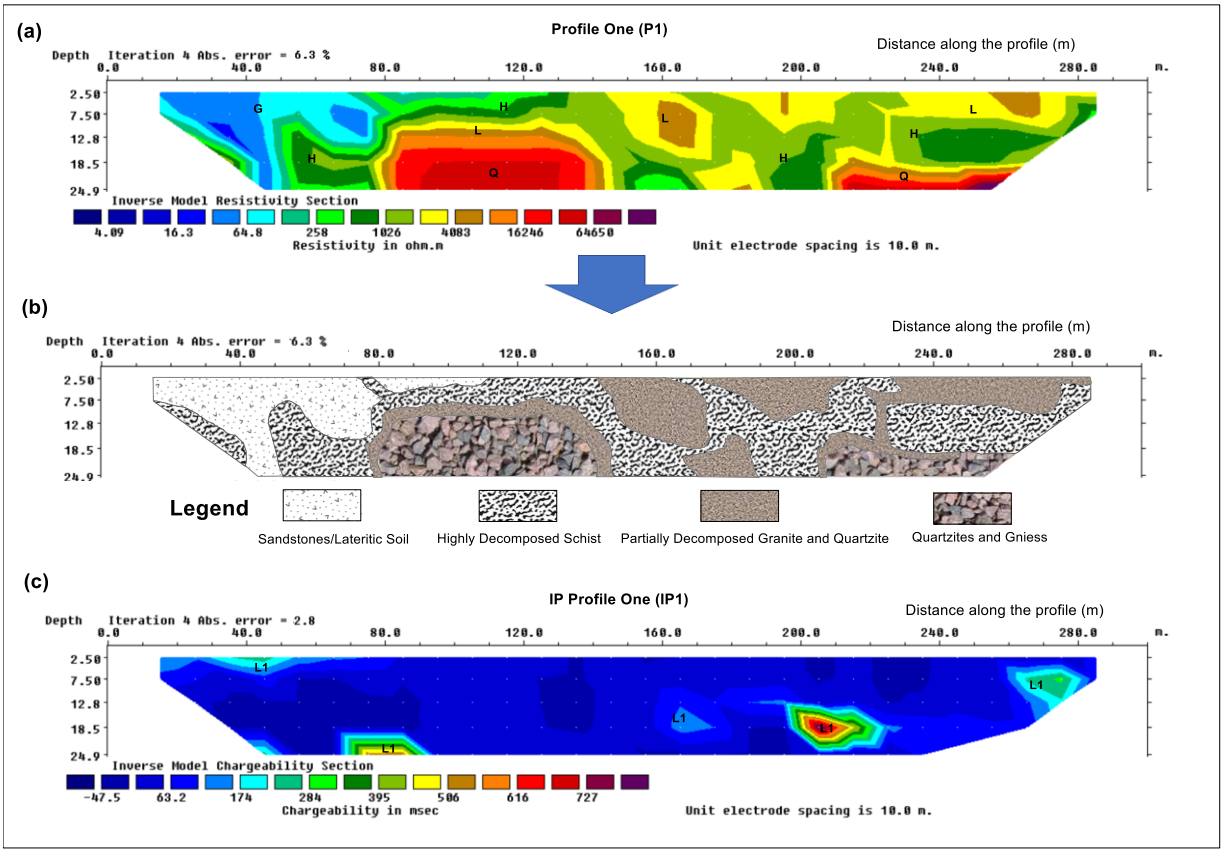

Fig. 8 **(a)** ERT model, **(b)** geologic section, and **(c)** IP section of the profile one.

partially decomposed. Locating the lithium pegmatite mineral may depend on the aforementioned rock formation's dyke subsurface structures. Figure 8(b) illustrates the further transformation of the inverse model section results, which are displayed in Figure 8(a), into a geologic section.

Figure 8(c) displays the chargeability sections along profile 1 (IP1) of the 2D inverse model results. The sections made it evident which regions—zone **L1**—showcase metallic minerals. The chargeability values ≥ 174 msec are most notable in these regions. It covers x-positions of 71-90 m, 190-220 m, 260-280 m, and 30-70 m at corresponding depths and thicknesses of 7.5 m, 18.5-24.9 m, 12.8-24.9 m, and 18.5 m. The higher chargeability of zone **L1** generally happens because of the collection of metallic minerals in host rocks of the study area. These targets could be considered as potential targets for the investigation into specific metallic minerals, particularly lithium pegmatite mineralisation.

3.3.2. GEOELECTRIC SECTIONS FOR PROFILE 2

Profile 2, which is 300 meters in lateral extent and positioned northwest to southeast (Fig. 9) is situated geographical coordinates; 10°48'7.2"N and 10°48'0"N as well as 4°45'0"E and 4°45'7.2"E (refer to Fig. 2). The differences in subsurface resistivity were divided into zones **G**, **H**, **L**, and **Q**. The subsurface variations for these zones are summarised in Table 2 with respect to the area's borehole lithology as provided in Table 1 and the resistivity of common rocks.

The key zones of likely lithium-bearing pegmatite mineralisation were found to be the zones of low and high resistivity (**G** and **L**). The low resistivity zone (**G**) may be the product of weathering in an oxidized rock, which is typically composed of Granite or Rhyolite, based on the geological setting of the research region. It might therefore be connected to specific minerals, especially Pegmatite which contains Lithium. Nevertheless, a high resistivity zone (**L**) produced the dyke formations that belong to Quartzite and partially decomposed Granite. These formations might be crucial for determining the presence of mineralisation, especially lithium mineralisation. These results from the resistivity section of Figure 9(a) were converted into the geologic section that is shown in Figure 9(b).

Figure 9(c) presents the chargeability section results of the profile two (IP2) 2D inverse model. Zone **L1** was the area with the potential for mineralisation that was most prominently displayed in this profile. Due to the host rocks' high concentration of metallic minerals, these areas tend to have higher chargeabilities. The depths and lateral distances that these zones (**L1**) occupies are shown in Table 2. These sites may be considered as potential research locations for specific metallic minerals, especially lithium pegmatite mineral.

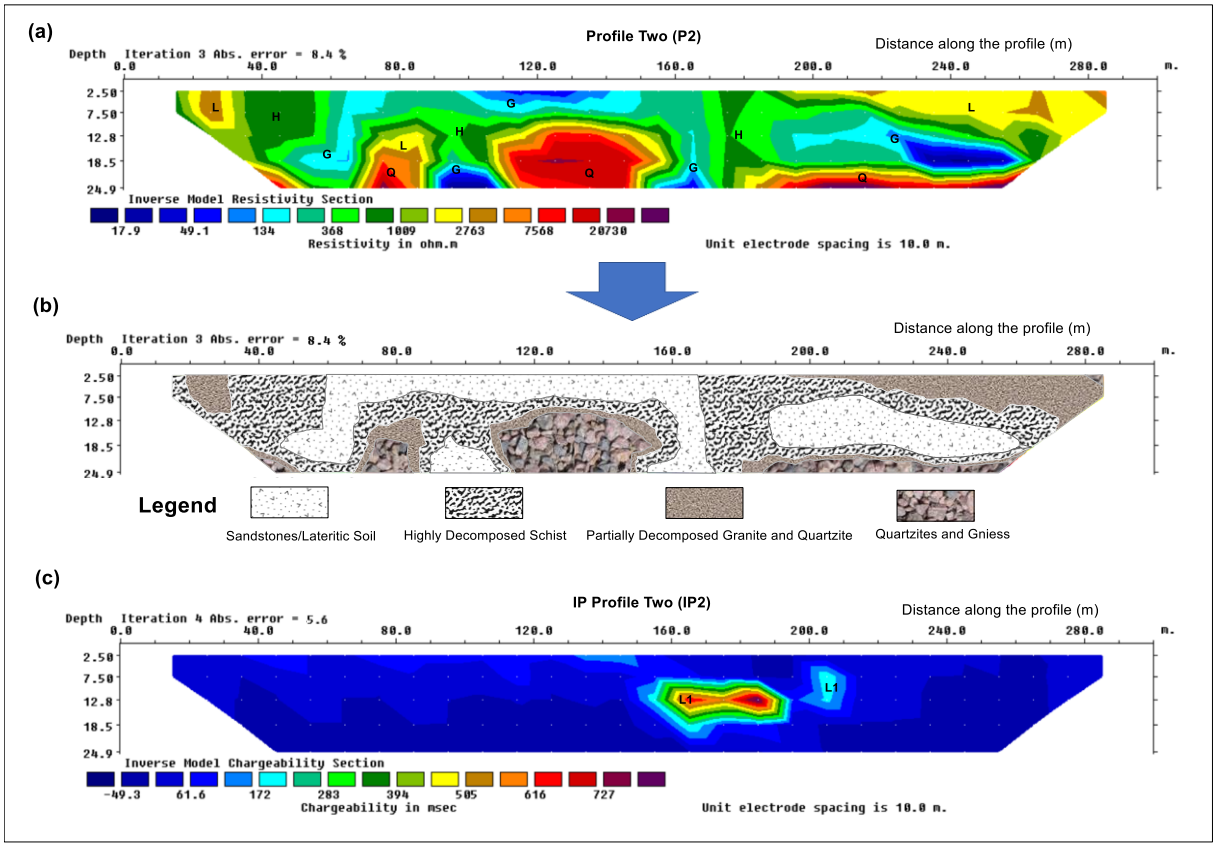

Fig. 9 **(a)** ERT model, **(b)** geologic section and **(c)** IP section of the profile two.

Table 2 A brief description of results from the combined use of the two geoelectric techniques.

Profile	Resistivity results				Induced polarisation results				Possible lithium-bearing pegmatite remarks
	Zone	Resistivity ranges (Ωm)	Lateral lengths (m)	Thickness/ Depth (m)	Zone	Chargeability ranges (msec)	Lateral lengths (m)	Thickness/ Depth (m)	
P1	**G**	4.009-64.8	0-80	12.8	L1	≥ 174	30-70, 71-90, 190-220 and 260-280	7.5, 185-24.9, 12.8-24.9 and 18.5	Yes
	H	64.9-1026	0-80	12.9-24.9	-	-	-	-	No
	L	1027-4083	140-170, 180-210 and 230-275	24.9, 12.8 and 7.5	-	-	-	-	Yes
	Q	4084-64650	80-140 and 220-260	24.9 and 18.5-24.9	-	-	-	-	No
P2	**G**	17.9-134	60-170, 90-110 and 190-260	7.5, 18.5-24.9 and 12.8-18.5	L1	174 and above	150-190 and 200-210	12.8-18.5 and 7.5-12.8	Yes
	H	135-1009	30-60, 70-160 and 170-190	18.5, 7.5-12.8 and 24.9	-	-	-	-	No
	L	1010-2763	20-30 and 200-300	12.8 and 12.8	-	-	-	-	Yes
	G	2764-20730	80-140 and 200-260	12.8-24.9 and 18.5-24.9	-	-	-	-	No

Table 3 Zones of potentially mineralised lithium bearing pegmatite in the area.

Profile No.	Lateral lengths (m)	Depth/ Thickness (m)	Geographic coordinate.				Locations
			Left End		Right End		
			Longitude	Latitude	Longitude	Latitude	
P1	30-90, 190-220 and 260-280.	7.5-24.9, 12.8-24.9 and 18.5.	4°51'2.16"E, 4°51'24.84"E and 4°51'37.8"E,	11°24'14.04"N, 11°23'42"N and 11°23'24"N,	4°51'9.72"E, 4°51'29.16"E and 4°51'41.4"E	11°24'3.24"N, 11°23'36.24"N and 11°23'19.68"N	Bajida
P2	150-190 and 200-210	12.8-18.5 and 7.5-12.8	4°52'6.6"E and 4°52'19.92"E	11°24'9.72"N and 11°23'51.72"N	4°52'11.28"E and 4°52'23.52"E	11°24'3.24"N and 11°23'47.4"N	Gonan Goli

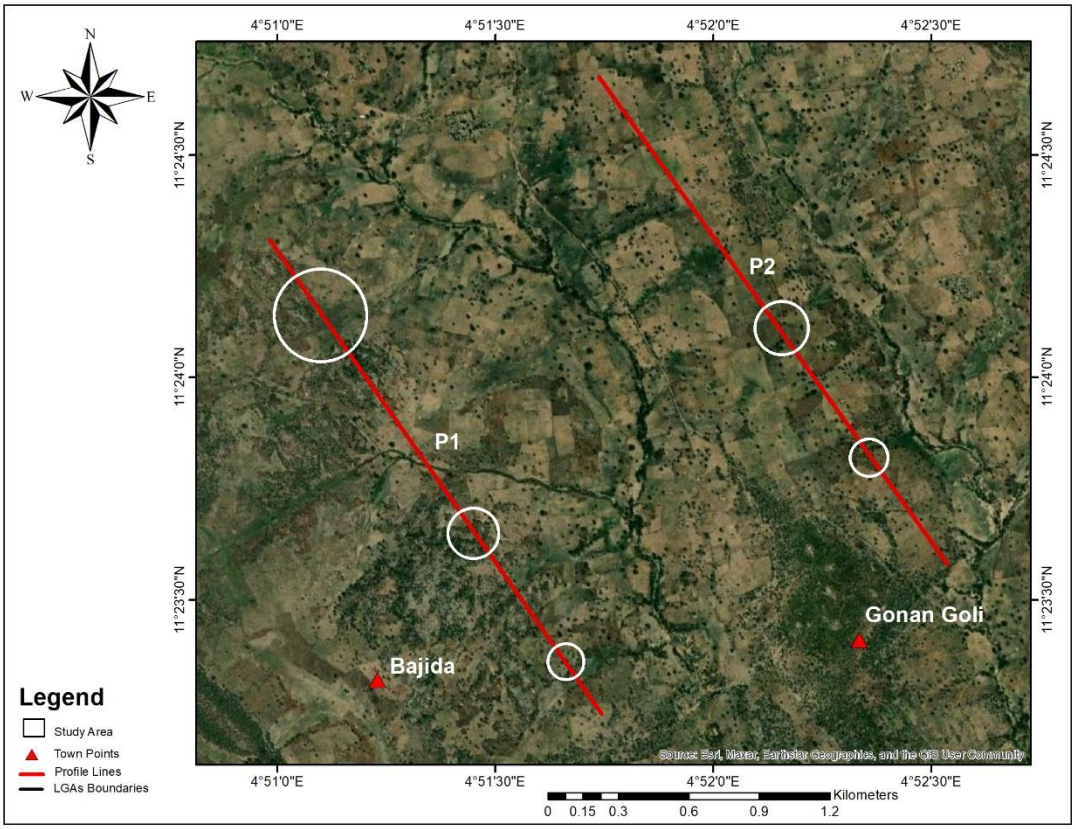

Fig. 10 Map of potential lithium-bearing pegmatite zones of the study area.

3.3.3. POTENTIAL ZONES OF LITHIUM-BEARING PEGMATITE IN THE AREA

Zones **G**, **L**, and **L1** represent the proposed integrated zones of lithium-bearing pegmatite mineral potential along geoelectric profiles 1 and 2 (P1 and P2 as well as IP1 and IP2). As seen in Figures 8–9, these zones are characterised by signatures of strong chargeability as well as low/high zones resistivity. The integrated key zones of lithium pegmatite mineralisation potential are shown in Table 3 (Fig. 10). These zones could be defined as the potential targets for lithium mineral exploration. The results of this study resulted in the creation of a database, which is shown in Tables 2 and 3, and contains the precise coordinates, lengths, and depths of prospective lithium pegmatite zones. This database could aid in locating lithium-bearing mineral-bearing regions for exploration purposes.

4. CONCLUSION

In conclusion, the used of integrated geophysical methods in this study reveals that hydrothermal alteration zones coupled with regions of the major magnetic structures (lineaments) could potentially be favourable for lithium-bearing pegmatite minerals. When related to the results in relation to geological setting of the area, the hydrothermally altered zones corresponding to high amplitude magnetic anomaly regions are associated with quartz gneiss, migmatitic augen gneiss, as well as moderate to fine-grained biotite. The regions of potential Li-mineral are located in Rijau, the eastern parts of Shanga, and Fakai. The locations were explored further using Geoelectric methods such as 2D ERT and IP thorough geophysical approaches. The results of the geoelectric method along P1 and P2 revealed the target zones of lithium-

bearing pegmatite mineralisation potential, which are zones **G**, **L**, and **L1**. These regions, which have low/high resistivity and chargeability signatures, could be defined as potential target zones for lithium pegmatite minerals of the study area. The areas of zones are located in Bajida and Gonan Goli of Kebbi state. The results of geoelectric techniques provided a database with accurate coordinates, lateral lengths, and thickness/depths for potential lithium-bearing pegmatite zones. This database could aid in the exploration of lithium-bearing pegmatites in the region. The study also backed up previous magnetic studies in the area by previous researchers. This study used both an aero-radiometric approach as well as an aeromagnetic technique to identify areas of the hydrothermally altered zone and regions with major structural features (lineaments) that could host lithium mineralisation, and the results were consistent with previous aeromagnetic studies of the area that only targeted magnetic structures and not the alteration zones.

ACKNOWLEDGEMENT

The authors would like to express their profound appreciation to the Tertiary Trust Fund (Tetfund) and the management of the Nigeria Geological Survey Agency (NGSA) for the release of the airborne magnetic and radiometric dataset. Our thanks are also extended to the district heads of Bajida and Gonan Goli of Kebbi State for approval of the site to collect geophysical data. Their appreciation also goes to the Department of Physics, Bayero University Kano for providing the instruments as well as Geosoft Inc. for the use of Oasis Montaj and Res2dinv Softwares.

REFERENCES

Adamu, L.M., Obaje, N.G., Sidi, A.A., Aweda, A.K. and Liman, H.M.: 2021, Geochemical evidence for the origin of the daranna manganese deposit, Kebbi state, Nigeria. Nig. J. Basic Appl. Sci., 29, 2, 30–45. DOI: 10.4314/njbas.v29i2.4

Adetona, A.A., Kwaghhua, F.I. and Aliyu, S.: 2022, Interpreting the magnetic signatures and radiometric indicators within Kogi State, Nigeria for economic resources. Geosyst. Geoenviron., 2, 100157. DOI: 10.1016/j.geogeo.2022.100157

Augie, A.I., Salako, K.A., Bery, A.A., Rafiu, A.A. and Jimoh, M.O.: 2024a, Integrated geophysical investigation using aero-radiometric and electrical methods for potential gold mineralization within Yauri/ Zuru schist belts, Kebbi State NW Nigeria. Earth Sci. Res. J., 28, 2, 137–146. DOI: 10.15446/esrj.v28n2.112066

Augie, A.I., Salako, K.A., Rafiu, A.A. and Jimoh, M.O.: 2024b, Integrated geophysical investigation for potential gold mineralised zone within lower part of Zuru schist belts, NW Nigeria. Nig. J. Phys., 33, 2, 1–14. DOI: 10.62292/njp.v33i2.2024.212

Augie, A.I., Salako, K.A., Rafiu, A.A. and Jimoh, M.O.: 2024c, Integrated 2D geoelectric prospecting for gold mineralization potential within southern part of Kebbi NW Nigeria. ANAS Trans. Earth Sci., 1, 180–202. DOI: 10.33677/ggianas20240100119

Augie, A.I., Salako, K.A., Rafiu, A.A. and Jimoh, M.O.: 2022a. Geophysical assessment for gold mineralisation potential over the southern part of Kebbi State using aeromagnetic data. Geol. Geophys. Environ., 48, 2, 177–193. DOI: 10.7494/geol.2022.48.2.177

Augie, A.I., Salako, K.A., Rafiu, A.A. and Jimoh, M.O.: 2022b, Geophysical magnetic data analyses of the geological structures with mineralisation potentials over the southern part of Kebbi, NW Nigeria. Min. Sci., 29, 179–203. DOI: 10.37190/msc222911

Balaram, V., Santosh, M., Satyanarayanan, M., Srinivas, N. and Gupta, H.: 2024, Lithium: A review of applications, occurrence, exploration, extraction, recycling, analysis, and environmental impact. Geosci. Front., 101868, 1674–987. DOI: 10.1016/j.gsf.2024

Barbosa, H., Amadeum, H., Soares, M.V.M., Pereira, E. and Freitas, R.: 2023, Lithium: A review on concentrations and impacts in marine and coastal systems. Sci. Total Environ., 857, 159374. DOI: 10.1016/j.scitotenv.2022.159374

Belgibayeva, A., Rakhmetova, A., Rakhatkyzy, M., Kairova, M., Mukushev, I., Issatayev, N., Kalimuldina, G., Nurpeissova, A., Sun, Y.K., and Bakenov, Z.: 2023, Lithium-ion batteries for low-temperature applications: Limiting factors and solutions. J. Power Sources, 557, 232550. DOI: 10.1016/j.jpowsour.2022.232550

Bonde, D.S., Lawali, S. and Salako, K.A.: 2019, Structural mapping of solid mineral potential zones over southern part of Kebbi state, northwestern Nigeria. J. Sci. Eng. Res., 6, 7, 229–240.

Bradley, D.C., Stillings, L.L., Jaskula, B.W., Munk, L. and McCauley, A.D.: 2017, Lithium. In critical mineral resources of the United States— economic and environmental geology and prospects for future supply. Geological Survey: Reston, K1–K21.

Core, D., Buckingham, A. and Belfield, S.: 2009, Detailed structural analysis of magnetic data-done quickly and objectively. SGEG Newsletter, 1, 2, 15–21.

Dickson, B.L. and Scott, K.M.: 1997, Interpretation of aerial gamma ray surveys-adding the geochemical factors. AGSO J. Aust. Geol. Geophys., 17, 2, 187–200.

Durrance, E.: 1986, Radioactivity in geology: principles and applications. Chichester: Ellis Horwood, 441.

Dzukogi, A.N. and Mahmud, M.B.: 2023, Mapping of potential lithium mineral deposits in some parts of Northwestern Nigeria using magnetic and Gamma-Ray Spectrometry data. African Journal of Environmental Sciences and Renewable Energy, 10, 1, 91–108.

Gourcerol, B., Gloaguen, E., Melleton, J., Tuduri, J. and Galiegue, X.: 2019, Re-assessing the European lithium resource potential—A review of hard-rock resources and metallogeny. Ore Geol. Rev., 109, 494–519. DOI: 10.1016/j.oregeorev.2019.04.015

Holden, E.J., Dentith, M. and Kavesi, P.: 2008, Towards the automatic analysis of regional aeromagnetic data to identify regions prospective for gold deposits. Computer Geoscience, 34, 1505–1513. DOI: 10.1016/j.cageo. 2007.08.007

Hoover, D.B. and Pierce, H.A.: 1990, Annotated bibliography of gamma-ray methods applied to gold exploration. U.S. Geol. Surv. Open-File Rep., 23, 90-203. DOI: 10.3133/ofr90203

Lawal, M.M., Salako, K.A., Abbas, M., Adewumi, T., Augie, A.I. and Khita, M.: 2021, Geophysical investigation of possible gold mineralization potential zones using a combined airborne magnetic data of lower Sokoto basin and its environs Northwestern Nigeria. International Journal of Progressive Sciences and Technologies (IJPSAT), 30, 1, 1-16. DOI: 10.52155

Lawali, S., Salako, K.A. and Bonde, D.S.: 2020, Delineation of mineral potential zones over lower part of Sokoto Basin, northwestern Nigeria using aeromagnetic data. Academic Research International (ARInt), 11, 2, 19–29.

Linnen, R.L., Samson, I.M., Jones, A.E.W. and Chakhmouradian, A.: 2014, Geochemistry of the rare-earth element, Nb, Ta, Hf, and Zr deposits: in treatise on geochemistry, 2nd ed. Elsevier, Amsterdam, The Netherlands, 543–568.

Linnen, R.L., Lichtervelde, M.V. and Cerny, P.: 2012, Granitic pegmatites as sources of strategic metals. Elements, 8, 4, 275–280. DOI: 10.2113/gselements.8.4.275

Loke, H.M.: 1999 Electrical imaging surveys for environment and engineering studies (practical guide to 2D and 3D survey). Earth Science, 44, 1, 131–152.

Loke, M.: 2000, Rapid least-square inversion of apparent resistivity pseudosections. Earth Sci., 64, 3, 31–52.

NGSA: 2006, Nigerian Geological Survey Agency, Nigeria.

Ohioma, J.O., Ezomo, F.O. and Akinsunmade, A.: 2017, Delineation of hydrothermally altered zones that favour gold mineralization in Isanlu area, Nigeria using aeroradiometric data**.** Int. Ann. Sci., 2, 1, 20-27. DOI: 10.21467/ias.2.1.20-27

Osazuwa, I.B. and Chii, E.C.: 2010, Two-dimensional electrical resistivity survey around the periphery of an artificial lake in the Precambrian basement complex of northern Nigeria. Int. J. Phys. Sci., 5, 3, 238–245.

Ramadan, T.M. and AbdelFattah, M.F.: 2010, Characterization of gold mineralization in Garin Hawal area, Kebbi State, NW Nigeria, using remote sensing. Egypt. J. Remote Sens. Space Sci., 13, 2, 153–163. DOI: 10.1016/j.ejrs.2009.08.001

Salako, K.A., Adetona, A.A., Rafiu, A.A., Augie, A.I., Jimoh, M.O., Alkali, A., Muriana, R.A. and Lawrence, J.O.: 2024, Integrated geophysical Investigation for gold mineralization potential over southern parts of Kebbi state and its environs, northwestern Nigeria. Heliyon, 10, 14, E34093. DOI: 10.1016/j.heliyon.2024.e34093

SARDA: 1988, Sokoto agricultural and rural development authority. Sokoto Fadama.

Wenqing, D., Lin D., Qingting L., Jinxiang, L. and Liyun, Z.: 2023, Lithium-rich pegmatite detection integrating high-resolution and hyperspectral satellite data in Zhawulong area, western Sichuan, China. Remote Sens., 15, 3969. DOI: 10.3390/rs15163969

Xiaobin, H., Nianzhi, L., Jinheng, F., Qingzhao, K. and Guixiong L.: 2015, Multi-electrode resistivity probe for investigation of local temperature inside metal shell battery cells via resistivity: experiments and evaluation of electrical resistance tomography. Energies, 8, 742–764. DOI: 10.3390/en8020742